JJMIE

Volume 12 Number 2, September. 2018
ISSN 1995-6665
Pages 99 - 107

Jordan Journal of Mechanical and Industrial Engineering

Pulsating Nanofluid Jet Impingement onto a Partially Heated Surface Immersed in a Porous Layer

Iman Zahmatkesh*, Seyyed Ali Naghedifar

Department of Mechanical Engineering, Mashhad Branch, Islamic Azad University, Mashhad, Iran

Received JAN 12 2018 *Accepted JULY 25 2018*

Abstract

Laminar forced convection heat transfer during pulsating nanofluid jet impingement onto a partially heated surface immersed in a porous layer is presented in this study. For this purpose, the Brinkman–extended Darcy model is adopted. The base fluid and the nanoparticles are taken to be in local thermal equilibrium with the same velocities and temperatures. The local thermal equilibrium is also assumed between the nanofluid and the porous matrix. Simulation results are validated thoroughly. Thereafter, the consequences of the pulsation frequency and amplitude, the Reynolds number, the Darcy number, the medium porosity, the nanoparticles fraction, and the geometric ratio on thermal performance of the system are analyzed. It is found that direct relations exist between the heat transfer rate and the pulsation amplitude, the medium porosity, the Darcy number, the nanoparticles fraction, and the geometric ratio whereas the pulsation frequency contributes neutrally. The presented results demonstrate that superimposing pulsation on the mean flow augments heat transfer as compared to an equivalent steady case.

Keywords: *Forced convection, Nanofluid, Porous media, Jet impingement, Pulsating flow.*

Nomenclature

A	pulsation amplitude
C	specific heat (J/(kg K))
d	half of the width of the jet inlet (m)
Da	Darcy number , κ/L^2
f	pulsation frequency (Hz)
h	height of the solution domain (m)
h	heat transfer coefficient (W/(m^2 K))
k	thermal conductivity (W/(m K))
L	half of the heat source length (m)
Nu	local Nusselt number, $\boldsymbol{h}L/k_f$
$\overline{Nu}$	space–averaged Nusselt number
$< \overline{Nu} >$	time–space–averaged Nusselt number
p	pressure (Pa)
P	dimensionless pressure, $p/(\rho_f V_0^2)$
Pe	Peclet number, $Pe = Re\ Pr$
Pr	Prandtl number, $\mu_f C_f/k_f$
Re	Reynolds number, $\rho_f V_0 L/\mu_f$
t	time (s)
T	temperature (K)
u, v	velocity components along x and $y$axes, respectively (m/s)
U, V	dimensionless velocity components, u/V_0 and v/V_0
V_0	mean inlet velocity (m/s)
w	half of the width of the solution domain (m)
x, y	Cartesian coordinates (m)
X, Y	dimensionless Cartesian coordinates, x/L and y/L

Greek Symbols

Θ	dimensionless temperature, $(T - T_C)/(T_H - T_C)$
κ	permeability (m^2)
μ	dynamic viscosity (Pa. s)
ρ	density (kg/m^3)
τ	dimensionless time, tV_0/L

* Corresponding author e-mail: zahmatkesh5310@mshdiau.ac.ir

  - Volume 12, Number 2 (ISSN 1995-6665)

ϕ	porosity
χ	nanoparticles fraction
ψ	stream function (m^2/s)
Ψ	dimensionless stream function, $\psi/V_0 L$
ω	vorticity $(1/s)$
Ω	dimensionless vorticity, $\omega L/V_0$
Subscripts	
C	cold
f	base fluid
H	hot
nf	nanofluid
p	nanoparticle
s	solid matrix
$stag$	stagnation point

1. Introduction

As a consequence of high rates of heat and mass transfer, impinging jets are widely used in industrial processes. Examples include cooling of electronic equipments and turbine blades, annealing of sheet metals, drying of paper, textile, and glass, and anti–icing systems. Thermal performance of impinging jets can be modified if one superimposes pulsation on the mean flow. This occurs since the pulsation redevelops and breaks up the boundary layers within each oscillation period, which may lead to thinner boundary layers as compared to an equivalent steady case. Previous studies indicate that there is a lack of consensus about the impact of flow pulsation on jet impingement heat transfer. Both improvement and deterioration of heat transfer due to creation of unsteady flows have been reported in the scientific literature. Additional studies are thereby required to examine the correlation between flow pulsation and heat transfer in impinging jets.

Addition of nanoparticles to conventional fluids is a recent way to improve cooling/heating performance. Physical reasoning for this behavior is the fact that thermal properties of the resulting fluid (nanofluid) are more proper than those of conventional fluids. Looking at the previous literature shows some recent interests on jet impingement heat transfer together with flow pulsation (e.g., [1–5]) or nanoparticles addition (e.g., [6–8]), separately. However, the combined effects have not been discussed thoroughly. The available work goes back to the study of Selimefendigil and Oztop [9]. They simulated pulsating jet impingement of an Al_2O_3–water nanofluid, and they studied the effects of the pulsation frequency along with the Reynolds number, and the nanoparticles fraction on the heat transfer characteristics. Their results led to the conclusion that in some cases, the combined effects of the flow pulsation and the inclusion of the nanoparticles may not be favorable for heat transfer augmentation.

Convective flows in porous media have been extensively analyzed in the past since many practical applications can be modeled with transport phenomena in porous media [10,11]. So, some researchers have discussed jet impingement cooling of heated surfaces immersed in porous media in the regimes of forced convection [12–14] and mixed convection [15–17]. Recently, thermal performance of jets impinging onto a solid heat source immersed in a porous layer has been analyzed by Saeid [18]. Meanwhile, Lam and Prakash [19] have studied jet impingement onto an array of heat sources mounted on a target surface with/without a porous layer. Local thermal non–equilibrium effects during jet impingement cooling of a constant–heat–flux plate have been considered by Buonomo et al. [20]. Oscillatory mixed convection in the jet impingement cooling of a horizontal surface immersed in a nanofluid–saturated porous medium has been simulated and discussed by Zahmatkesh and Naghedifar [21]. More recently, Chinige et al. [22] have reported an optimized configuration of multijets impinging through porous passages.

Although previous achievements are important, the combined effects of flow pulsation, nanoparticles addition, and porous media in jet impingement heat transfer have not been analyzed yet. In the present contribution, laminar forced convection heat transfer during pulsating nanofluid jet impingement onto a partially heated surface immersed in a porous layer is simulated. Thereafter, the consequences of the pertinent parameters on thermal performance of this complex system are discussed. The current parameters include the pulsation frequency and amplitude, the Reynolds number, the Darcy number, the medium porosity, the nanoparticles fraction, and the geometric ratio.

2. Mathematical Modeling

2.1. Physical model

As depicted in Fig. 1, the present computational domain consists of a channel including two parallel plates separated with a distance h. A nanofluid jet from a slot on the top adiabatic plate with a width of $2d = 0.5L$ flows through a saturated porous layer and impinges onto the bottom plate that is partially heated. Subsequently, it flows out through the outlets, which are located at $2w = 25L$ far from each other along the plates. The pulsating inlet jet has a time dependent velocity distribution while its temperature (T_C) is smaller than that of the heated section of the channel (T_H). It is assumed that temperature difference between the incoming fluid and the isothermal plate is not significant. Therefore, buoyancy effects are ignored. Additionally, the nanofluid properties are taken temperature–independent.

2.2. Nanofluid description

In this study, the basefluid is water with Al_2O_3 nanoparticles which are added in 1, 4, and 8 percent by volume. The nanofluid flow is assumed to be Newtonian, incompressible, and laminar with negligible viscous dissipation. The base fluid and the nanoparticles are taken to be in local thermal equilibrium with the same velocities

and temperatures. The local thermal equilibrium is also assumed between the nanofluid and the porous matrix. Consequently, a single–phase approach is used for the simulation of the flow field. Thermophysical properties of the base fluid and the nanoparticles are kept constant at 300K with the numerical values reported in [23]. Effective properties of the nanofluid are determined as follows:

Density:

$$\rho_{nf} = (1-\chi)\rho_f + \chi\rho_p \tag{1}$$

Specific heat:

$$(\rho C)_{nf} = (1-\chi)(\rho C)_f + \chi(\rho C)_p \tag{2}$$

Dynamic viscosity [24]:

$$\mu_{nf} = \frac{\mu_f}{(1-\chi)^{2.5}} \tag{3}$$

Thermal conductivity [25]:

$$\frac{k_{nf}}{k_f} = \frac{(k_p + 2k_f) - 2\phi(k_f - k_p)}{(k_p + 2k_f) + \phi(k_f - k_p)} \tag{4}$$

2.3. Governing equations

Governing equations for the problem at hand are [26]:

Continuity equation:

$$\frac{\partial u}{\partial x} + \frac{\partial v}{\partial y} = 0 \tag{5}$$

Momentum equations:

$$\rho_{nf}\left[\frac{1}{\phi}\frac{\partial u}{\partial t} + \frac{1}{\phi^2}\left(u\frac{\partial u}{\partial x} + v\frac{\partial u}{\partial y}\right)\right] = -\frac{\partial p}{\partial x} + \frac{\mu_{nf}}{\phi}\left(\frac{\partial^2 u}{\partial x^2} + \frac{\partial^2 u}{\partial y^2}\right) - \frac{\mu_{nf}}{\kappa}u \tag{6}$$

$$\rho_{nf}\left[\frac{1}{\phi}\frac{\partial v}{\partial t} + \frac{1}{\phi^2}\left(u\frac{\partial v}{\partial x} + v\frac{\partial v}{\partial y}\right)\right] = -\frac{\partial p}{\partial y} + \frac{\mu_{nf}}{\phi}\left(\frac{\partial^2 v}{\partial x^2} + \frac{\partial^2 v}{\partial y^2}\right) - \frac{\mu_{nf}}{\kappa}v \tag{7}$$

Energy equation:

$$(\rho C)_{nf}\left(\frac{\partial T}{\partial t}\right) + (\rho C)_{nf}\left(u\frac{\partial T}{\partial x} + v\frac{\partial T}{\partial y}\right) = k_{nf}\left(\frac{\partial^2 T}{\partial x^2} + \frac{\partial^2 T}{\partial y^2}\right) \tag{8}$$

Here, the Forchheimer term has been ignored in the momentum equations. The following parameters are used to make the above equations dimensionless:

$$\tau = \frac{t}{L/V_0} \quad X = \frac{x}{L} \quad Y = \frac{y}{L} \quad U = \frac{u}{V_0} \quad V = \frac{v}{V_0} \quad P = \frac{p}{\rho_f V_0^2} \quad \Theta = \frac{T - T_C}{T_H - T_C} \tag{9}$$

The resulting momentum equations are thereafter cross–differentiated and then subtracted. So that, the pressure terms are removed. Consequently, one obtains the dimensionless governing equations in terms of stream function (Ψ) and vorticity (Ω) as:

Continuity equation:

$$\frac{\partial^2 \Psi}{\partial X^2} + \frac{\partial^2 \Psi}{\partial Y^2} = -\Omega \tag{10}$$

Momentum equation:

$$\frac{1}{\phi}\frac{\partial \Omega}{\partial \tau} + \frac{1}{\phi^2}\left(\frac{\partial \Psi}{\partial Y}\frac{\partial \Omega}{\partial X} - \frac{\partial \Psi}{\partial X}\frac{\partial \Omega}{\partial Y}\right) = \frac{1}{\phi\, Re}\frac{\rho_f}{\rho_{nf}}\frac{\mu_{nf}}{\mu_f}\left(\frac{\partial^2 \Omega}{\partial X^2} + \frac{\partial^2 \Omega}{\partial Y^2}\right) - \frac{1}{Re\, Da}\frac{\rho_f}{\rho_{nf}}\frac{\mu_{nf}}{\mu_f}\Omega \tag{11}$$

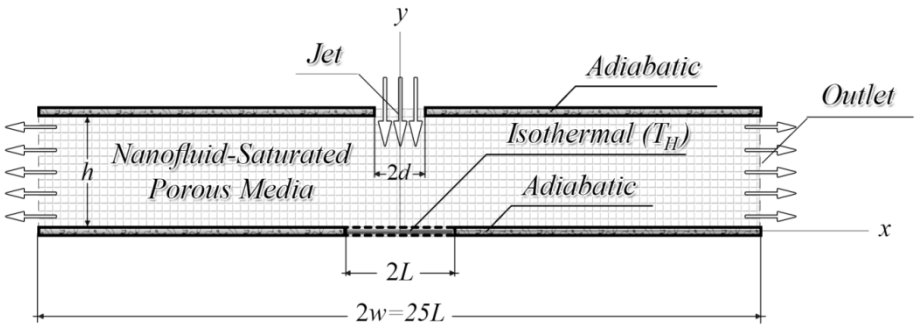

Figure 1: Schematic of the jet impingement problem.

Energy equation:

$$\frac{\partial \Theta}{\partial \tau}+\frac{\partial \Psi}{\partial Y}\frac{\partial \Theta}{\partial X}-\frac{\partial \Psi}{\partial X}\frac{\partial \Theta}{\partial Y} = \frac{1}{Re\ Pr_f}\frac{k_{nf}}{k_f}\frac{(\rho C)_f}{(\rho C)_{nf}}\left(\frac{\partial^2 \Theta}{\partial X^2}+\frac{\partial^2 \Theta}{\partial Y^2}\right) \quad (12)$$

with:

$$Re=\frac{\rho_f V_0 L}{\mu_f} \qquad Da=\frac{\kappa}{L^2} \qquad Pr_f=\frac{\mu_f C_f}{k_f} \quad (13)$$

2.4. Boundary conditions

The current flow problem is symmetric about the $y$axes. So, the right side of Fig. 1 is selected as the computational domain. The incoming nanofluid is assumed to have a uniform but time–dependent velocity profile with the form of $V=1+A\sin(2\pi f\tau)$ and a constant temperature. Moreover, the fully–developed condition is prescribed at the outlet for the velocity and temperature. The associated boundary conditions are:

At the inlet$(0<X<d/L, Y=h/L)$:

$$\Psi=X[1+A\sin(2\pi f\tau)] \qquad \Omega=-\frac{\partial^2 \Psi}{\partial Y^2} \qquad \Theta=0 \quad (14a)$$

At the outlet $(X=w/L, 0<Y<h/L)$:

$$\frac{\partial \Psi}{\partial X}=0 \qquad \frac{\partial \Omega}{\partial X}=0 \qquad \frac{\partial \Theta}{\partial X}=0 \quad (14b)$$

At the symmetry axis $(X=0, 0<Y<h/L)$*:*

$$\frac{\partial \Psi}{\partial Y}=0 \qquad \frac{\partial \Omega}{\partial X}=0 \qquad \frac{\partial \Theta}{\partial X}=0 \quad (14c)$$

At the upper adiabatic surface $(d/L\le X\le w/L, Y=h/L)$*:*

$$\Psi=\frac{d}{L}=0.25 \qquad \Omega=-\frac{\partial^2 \Psi}{\partial Y^2} \qquad \frac{\partial \Theta}{\partial Y}=0 \quad (14d)$$

At the heater $(0<X<1, Y=0)$*:*

$$\Psi=0 \qquad \Omega=-\frac{\partial^2 \Psi}{\partial Y^2} \qquad \Theta=1 \quad (14e)$$

At the lower adiabatic surface $(1\le X\le w/L, Y=0)$*:*

$$\Psi=0 \qquad \Omega=-\frac{\partial^2 \Psi}{\partial Y^2} \qquad \frac{\partial \Theta}{\partial Y}=0 \quad (14f)$$

To ensure that the lower surface is large enough to satisfy the fully–developed boundary condition at the outlet, the computational domain is doubled in the longitudinal direction. Inspection of the results demonstrates that such a change may not bring substantial variations in the simulation results.

2.5. Nusselt number

In this paper, heat transfer performance of the pulsating nanofluid jet is evaluated using the Nusselt number. To this aim, the local Nusselt number, the space–averaged Nusselt number, and the time–space–averaged Nusselt number are employed. The local Nusselt number is defined as:

$$Nu = -\frac{k_{nf}}{k_f}\left(\frac{\partial \Theta}{\partial Y}\right)_{Y=0} \tag{15}$$

The space–averaged Nusselt number at each time instant is obtained after integrating the local Nusselt number along the heater:

$$\overline{Nu} = \int_0^1 Nu.\, dX \tag{16}$$

One arrives at the time–space–averaged Nusselt number by applying time–averaging to the space–averaged Nusselt number, i.e.,

$$< \overline{Nu} >= \frac{1}{\tau}\int_0^\tau \overline{Nu}.\, d\tau \tag{17}$$

3. Solution procedure

3.1. The CFD code

Solution of the unsteady governing equations is accomplished using an implicit finite–difference approach. The diffusion terms are descretized by a second–order central–difference method while a second–order upwind scheme is applied to the convective terms. A computer code was developed in FORTRAN to perform the current calculations.

Schematic of the current non–uniform grid system is depicted in Fig. 2. Notice that the grid points are clustered at the proximity of the header as well as the upper and lower surfaces.

To undertake a grid independency study, the lower plate is maintained at a constant temperature while the remaining parameters are assumed to be $Re = 100, \chi = 0.06, Da = \infty$, and $\phi = 1$. Thereafter, numerical values of the local Nusselt number for different grid systems including $80 \times 27, 120 \times 40, 180 \times 60, 270 \times 90,$ and 405×105 are compared. It is found that a 270×90 grid system provides acceptable results since difference in the values of $\overline{Nu}$ employing 270×90 and 405×105 grids remains below 2%.

In order to find suitable time–step, results in terms of temporal variations of the Nusselt number at the stagnation point for different time–steps are compared in Fig. 3. It is obvious that the cases with $\Delta\tau \leq 0.5 \times 10^{-4}$ lead to nearly identical results. So, $\Delta\tau = 0.5 \times 10^{-4}$ is chosen for our forthcoming calculations.

3.2. Validation study

The current computational code is a modified version of an in–house code built and validated in the previous works [27–29]. In order to validate this code for the simulation of the current jet impingent problem, we compare our results with those of Wong and Saeid [16] and Sivasamy et al. [17] in Figs. 4 and 5, respectively. The study of Sivasamy et al. [17] has considered a constant–heat–flux heater in unsteady regime while Wong and Saeid [16] have simulated an isothermal heater in steady conditions. To validate the current nanofluid model in porous media, simulation results for natural convection of anAl_2O_3–water nanofluid with $\chi = 0.1$ are compared with those of Bourantas et al. [30] in Fig. 6 for two different Darcy numbers. The obvious agreement between the results of the current code and those of the previous studies assures us that the current mathematical model and solution procedure are accurate and lends confidence into the simulation results to be presented subsequently.

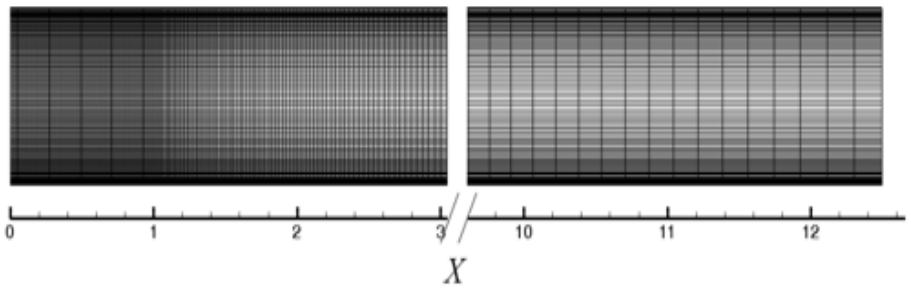

Figure 2: Distribution of the grid points in the solution domain.

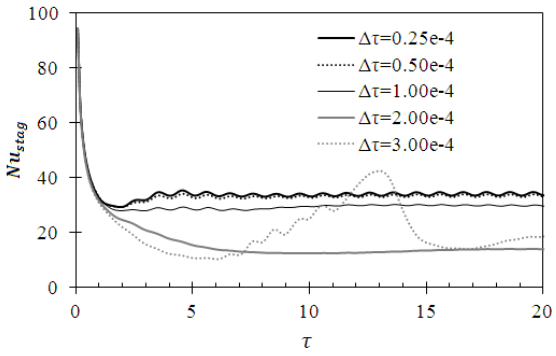

Figure 3: Time–step study ($Re = 400, Da = \infty, \chi = 0.06, \phi = 1.0$).

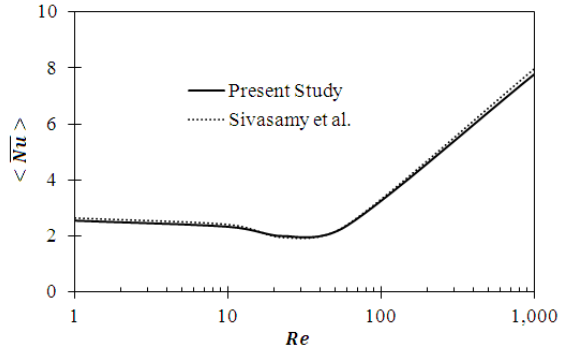

Figure 5: Comparing the present results with those of Sivasamy et al. [17]

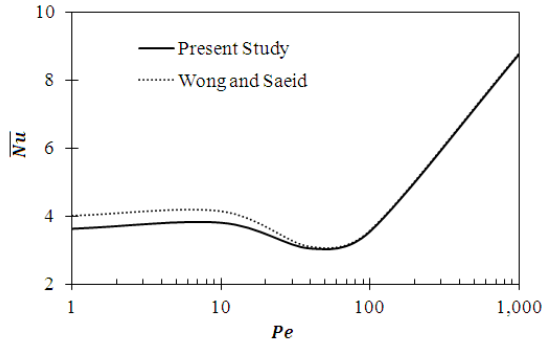

Figure 4: Comparing the present results with those of Wong and Saeid [16]

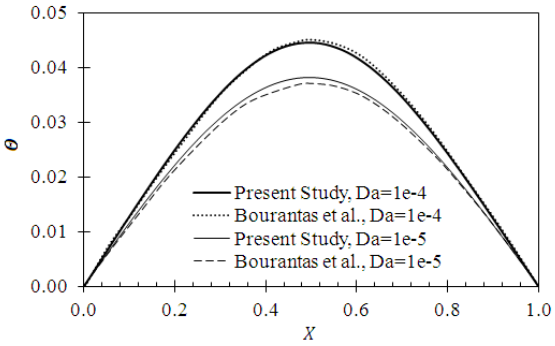

Figure 6: Comparing the present results with those of Bourantas et al. [29]

4. Simulation results

In this section, simulation results are presented and discussed. To provide a picture about the consequences of the pertinent parameters, computations are undertaken for a range of the pulsation frequency and amplitude ($1 \le f \le 2$ and $0.5 \le A \le 1$), the Reynolds number ($200 \le Re \le 800$), the medium porosity ($0.6 \le \phi \le 0.8$), the Darcy number ($10^{-5} \le Da \le 10^{-1}$), the nanoparticles fraction ($0.01 \le \chi \le 0.08$), and the geometric ratio ($0.5 \le L/h \le 2.0$). In all cases, a constant Prandtl number is assumed for the base fluid with $Pr_f = 6.2$. Moreover, *Base Case* is considered as $f = 0$ (steady–state), $Re = 400$, $\phi = 0.7, Da = 10^{-3}$, $\chi = 0.04$, and $L/h = 1$ in order to be compared with other results.

4.1. Effects of the pulsation frequency and amplitude

Firstly, the effects of the pulsation frequency and amplitude on thermal behavior of the current flow problem are analyzed. To this aim, computations are undertaken for different values of these parameters maintaining other pertinent parameters identical to the base case. Results in terms of temporal variations of $\overline{Nu}$ for $45 \le \tau \le 50$ are plotted in Fig. 7. The corresponding time–space–averaged Nusselt numbers are also reported in Table 1. The present selection of the time interval ensures us to reach stable oscillations.

Inspection of the presented results indicates that duplicating the pulsation amplitude leads to about 6% elevation in $< \overline{Nu} >$. This trend is consistent with previous results of Demircan and Turkoglu [1] and Geng et al. [3]. Notice also that increase in the pulsation frequency, in spite of changing the oscillation pattern, has not produced noticeable rise in the time–space–averaged Nusselt number under the current circumstances.

Comparing the results of the pulsating cases with those of the base case (i.e., steady–state) indicates that, in the present cases, the sinusoidal inlet velocity provides higher heat transfer rates. This is attributed to the fact that the flow pulsation redevelops and breaks up the boundary layers in a continuous manner. So, thinner boundary layers with higher heat transfer coefficients establish in a pulsating case as compared to an equivalent steady one.

4.2. Effect of the Reynolds number

Next, the impact of the Reynolds number is assessed. Accordingly, simulation results in terms of numerical values of $< \overline{Nu} >$ for different Reynolds numbers are provided in Table 2. The presented results correspond to $A = 0, 0.5$, and 1. Results investigation clearly indicates that the jet impingement heat transfer is a strong function of the Reynolds number. This is in accord with the results of Jeng and Tzeng [12] and is expected since Re is directly related to the flow momentum. Closer scrutiny of the presented results demonstrates up to about 63% rise in heat transfer as a consequence of passing from $Re = 400$ to $Re = 800$. This allows one to conclude that the consequence of the Reynolds number is more prominent than that of the pulsation frequency and amplitude. Notice also that, the effect of A on $< \overline{Nu} >$ becomes more remarkable as the Reynolds number increases. Heat transfer improvements as a result of

duplication of A are about 3, 6, and 9 percent for the Reynolds numbers of 200, 400, and 800, respectively.

4.3. Effect of the medium porosity

Table 3 is constructed to show the effect of the medium porosity on the time–space–averaged Nusselt number. Here, three values of the porosity (i.e., $\phi = 0.6, 0.7,$ and 0.8) are compared. Clearly, the rise of porosity from 0.7 to 0.8 has increased the Nusselt values up to about 8%. The trend of the Nusselt rise due to increase in the medium porosity has been previously reported by Wong and Saeid [16] and occurs due to reduction in the thickness of thermal boundary layer.

4.4. Effect of the Darcy number

It is interesting to investigate the consequences of the Darcy number on the heat transfer performance of the impinging jet. To this aim, temporal variations of $\overline{Nu}$ for different Darcy numbers are shown in Fig. 8. The figure indicates heat transfer enhancement as a result of increase in the Darcy number. This is expected due to decrease in the frictional resistance of the medium. It is noteworthy that at the smallest Darcy number (i.e., $Da = 10^{-5}$), the results coincide with those of $Da = 10^{-3}$. So, they are omitted from the figure for the sake of brevity.

4.5. Effect of the nanoparticles fraction

Effect of the nanoparticles fraction on the heat transfer performance is demonstrated in Fig. 9. The figure indicates that increase in the nanoparticles fraction enhances the jet impingement heat transfer. This occurs as a consequence of improvement in thermophysical properties of the nanofluid and is in agreement with previous evidences of Dutta et al. [6], Torshizi and Zahmatkesh [7], and Lam and Prakash [8].

4.6. Effect of geometric ratio

Geometric ratio is defined here as the proportion of the half of the heater length to the jet–to–plate spacing (i.e., L/h). So, increase in L/h can be interpreted as narrowing the distance between the jet and the target surface. Figure 10 shows the effect of this parameter on temporal variations of the space–averaged Nusselt number. Notice that as the geometric ratio increases, the numerical values of $\overline{Nu}$ enhance. The observed behavior is in accord with previous findings of Saeid and Mohamad [15] and Sivasamy et al. [17]. Substantial increase in the pulsation amplitude appears in the highest geometric ratio (i.e., $L/h = 2$)). For $L/h = 0.5$, however, the oscillations are roughly disappeared and the Nusselt numbers decrease. This occurs since under this circumstance, the pulsating jet and the target surface are far apart that decreases the velocity magnitudes and the flow pulsation at the proximity of the heater. Closer scrutiny of the figure demonstrates that in the case with $L/h = 0.5$, the heat transfer of the pulsating jet is even weaker than that of the base case (i.e., steady–state jet with $L/h = 1$).

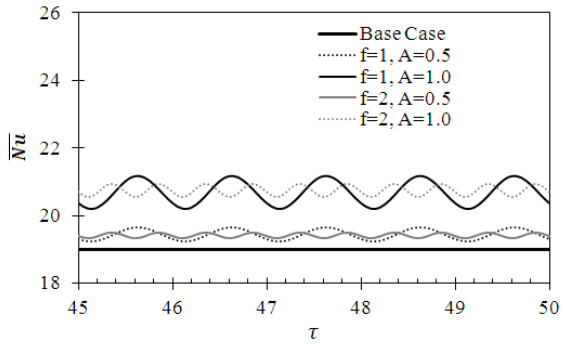

Figure 7: Effects of the pulsation frequency and amplitude on the temporal variations of the space–averaged Nusselt number.

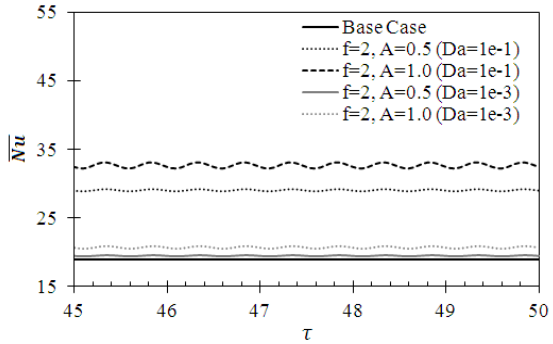

Figure 8: Effect of the Darcy number on the temporal variations of the space–averaged Nusselt number.

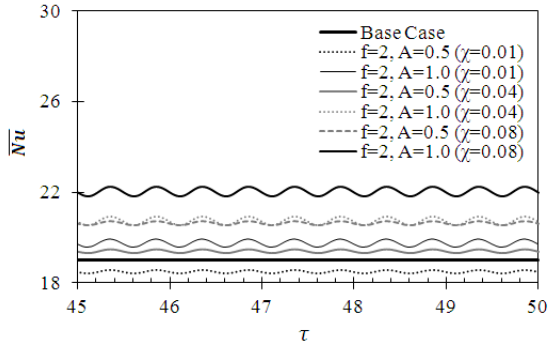

Figure 9: Effect of the nanoparticles fraction on the temporal variations of the space–averaged Nusselt number.

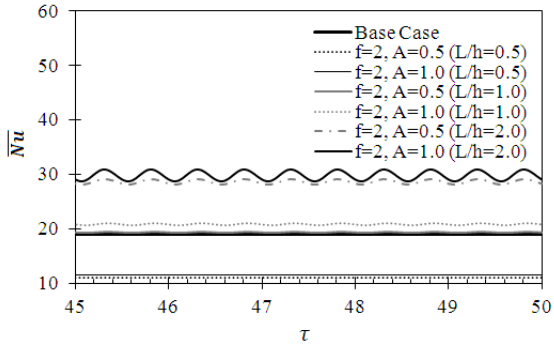

Figure 10: Effect of the geometric ratio on the temporal variations of the space–averaged Nusselt number.

Table 1. Effects of the pulsation frequency and amplitude on the time–space–averaged Nusselt number.

f	A	$< \overline{Nu} >$
0	0	19.9
1	0.5	20.3
1	1	21.5
2	0.5	20.3
2	1	21.6

Table 2. Effect of the Reynolds number on the time–space–averaged Nusselt number.

f	A	Re	$< \overline{Nu} >$
0	0	400	19.9
2	0.5	200	13.9
2	1	200	14.3
2	0.5	400	20.3
2	1	400	21.6
2	0.5	800	32.0
2	1	800	35.4

Table 3. Effect of the medium porosity on the time–space–averaged Nusselt number.

f	A	ϕ	$< \overline{Nu} >$
0	0	0.7	19.9
2	0.5	0.6	19.5
2	1	0.6	20.4
2	0.5	0.7	20.3
2	1	0.7	21.6
2	0.5	0.8	21.5
2	1	0.8	23.3

5. Concluding remarks

Based on the presented results, the following conclusions may be drawn:

1. Superimposing pulsation on the mean flow augments heat transfer as compared to an equivalent steady case.
2. Increase in the pulsation amplitude leads to heat transfer improvement, especially in higher Reynolds numbers.
3. Growth of the pulsation frequency, in spite of changing the oscillation pattern, may not produce noticeable rise in the time–space–averaged Nusselt number.
4. With increase in the Reynolds number, the medium porosity, the Darcy number, the nanoparticles fraction, and the geometric ratio, higher cooling performance can be achieved.

References

[1] T. Demircan, H. Turkoglu, "The numerical analysis of oscillating rectangular impinging jets". Numerical Heat Transfer, Part A, Vol. 58(2010)146–161.

[2] S. Alimohammadi, D.B. Murray, T. Persoons, "On the numerical–experimental analysis and scaling of convective heat transfer to pulsating impinging jets". International Journal of Thermal Sciences, Vol. 98 (2015)296–311.

[3] L. Geng, C. Zheng, J. Zhou, "Heat transfer characteristics of impinging jets: The influence of unsteadiness with different waveforms". International Communicationsin Heat and Mass Transfer, Vol. 66 (2015) 105–113.

[4] G. Eschmann, A. Kuntze, W. Uffrecht, E. Kaiser, S. Odenbach, "Experimental and numerical investigation of heat transfer coefficients in gaseous impinging jets– First test of a recent sensor concept for steady and unsteady flow".International Journal of Thermal Sciences, Vol. 96 (2015) 290–304.

[5] S. Ghadi, K. Esmailpour, M. Hosseinalipour, M. Kalantar, "Dynamical study of pulsed impinging jet with time varying heat flux boundary condition".Heat Transfer– Asian Research, Vol. 45 (2016) 85–100.

[6] E. Torshizi, I. Zahmatkesh, "Comparison between single–phase, two–phase mixture, and Eulerian–Eulerian models for the description of jet impingement of nanofluids". Journal of Applied & Computational Sciences in Mechanics, Vol. 27(2016) 55–70.

[7] P. Naphon, L. Nakharintr, S. Wiriyasart, "Continuous nanofluids jet impingement heat transfer and flow in a micro–channel heat sink". International Journal of Heat and Mass Transfer, Vol. 126 (2018) 924–932.

[8] F. Selimefendigil, H.F. Oztop, "Analysis and predictive modeling of nanofluid–jet impingement cooling of an isothermal surface under the influence of a rotating cylinder". International Journal of Heat and Mass Transfer, Vol. 121 (2018) 233–245.

[9] F. Selimefendigil, H.F. Oztop, "Pulsating nanofluids jet impingement cooling of a heated horizontal surface".International Journal of Heat and Mass Transfer, Vol. 69 (2014) 54–65.

[10] S.R. Kumar,"The effect of the couple stress fluid flow on MHD peristaltic motion with uniform porous medium in the presence of slip effect". Jordan Journal of Mechanical and Industrial Engineering, Vol. 9 (2015) 269–278.

[11] K. Singh, M. Kumar,"The effect of chemical reaction and double stratification on MHD free convection in a micropolar fluid with heat generation and Ohmic heating". Jordan Journal of Mechanical and Industrial Engineering, Vol. 9 (2015) 279–288.

[12] T.M. Jeng, S.C. Tzeng, "Numerical study of confined slot jet impinging on porous metallic foam heat sink".International Journal of Heat and Mass Transfer, Vol. 48 (2005) 4685–4694.

[13] D.R. Graminho, M.J.S. de Lemos, "Laminar confined impinging jet into a porous layer". NumericalHeat Transfer, Part A, Vol. 54 (2008) 151–177.

[14] M.J.S. de Lemos, C. Fischer, "Thermal analysis of an impinging jet on a plate with and without a porous layer". Numerical Heat Transfer, Part A, Vol. 54 (2008) 1022–1041.

[15] N.H. Saeid, A.A. Mohamad, "Jet impingement cooling of a horizontal surface in a confined porous medium: Mixed convection regime". International Journal of Heat and Mass Transfer, Vol. 49 (2006)3906–3913.

[16] K.C. Wong, N.H. Saeid, "Numerical study of mixed convection on jet impingement cooling in a horizontal porous layerusing Brinkman–extended Darcy model".International Journal of Thermal Sciences, Vol. 48 (2009) pp. 96–104.

[17] A. Sivasamy, V. Selladurai, P.R. Kanna, "Mixed convection on jet impingement cooling of a constant heat flux horizontal porous layer".International Journal of Thermal Sciences, Vol. 49 (2010) pp. 1238–1246.

[18] N.H. Saeid, "Mixed convection jet impingement cooling of a rectangular solid heat source immersed in a porous layer". Journal of Porous Media, Vol. 18 (2015)pp. 401–413.

[19] P.A.K. Lam, K.A.P. Prakash, "A numerical investigation of heat transfer and entropy generation during jet impingement cooling of protruding heat sources without and with porous medium". Energy Conversion & Management, Vol. 89 (2015) pp. 626–643.

[20] B. Buonomo, G. Lauriat, O. Manca, S. Nardini, "Numerical investigation on laminar slot–jet impingement in a confined porous medium in local thermal non–equilibrium".International Journal of Heat and Mass Transfer, Vol. 98 (2016) pp. 484–492.

[21]I. Zahmatkesh, S.A. Naghedifar, "Oscillatory mixed convection in the jet impingement cooling of a horizontal surface immersed in a nanofluid–saturated porous medium". Numerical Heat Transfer, Part A,Vol. 72 (2017) 401–416.

[22] S.K. Chinige, N. Ghanta, A. Pattamatta, "Multiobjective optimization study of jet impingement heat transfer through a porous passage configuration". Numerical Heat Transfer, Part A,Vol. 73 (2018) 446–465.

[23] I. Zahmatkesh, "On the suitability of volume–averaging approximation for the description of thermal expansion coefficient of nanofluids".Proceedings of the Institution of Mechanical Engineering, Part C: Journal of Mechanical Engineering Science, Vol. 229 (2015)pp. 2835–2841.

[24] H.C. Brinkman, "The viscosity of concentrated suspensions and solutions". Journal of Chemical Physics, Vol. 20 (1952)pp. 571–581.

[25] J.C. Maxwell–Garnett, "Colours in metal glasses and in metallic films". Philosophical Transactions of the Royal Society of London, Series A, Vol. 203 (1904) 385–420.

[26] Nield DA, Bejan A. Convection in porous media. 4th ed. New York; Springer–Verlag, 2013.

[27] I. Zahmatkesh, "On the importance of thermal boundary conditions in heat transfer and entropy generation for natural convection inside a porous enclosure".International Journal of Thermal Sciences, Vol. 47 (2008)339–346.

[28] I. Zahmatkesh, "Effect of a thin fin on natural convection heat transfer in a thermally stratified porous layer". Emirates Journal for Engineering Research, Vol. 19 (2014) 57–64.

[29] I. Zahmatkesh, "Heatline visualization for buoyancy–driven flow inside a nanofluid–saturated porous enclosure".Jordan Journal of Mechanical and Industrial Engineering, Vol. 9 (2015) 149–157.

[30] G.C. Bourantas, E.D. Skouras, V.C. Loukopoulos, V.N. Burganos, "Heat transfer and natural convection of nanofluids in porous media".European Journalof Mechanics B/Fluids, Vol. 43 (2014) 45–56.